# Observer-Based De-Convolution of Deterministic Input in Coprime Multi-Channel Systems with Its Application to Non-Invasive Central Blood Pressure Monitoring

Zahra Ghasemi
Department of Mechanical Engineering, University of Maryland, College Park, MD 20742, USA
2107B Glenn L. Martin Hall, University of Maryland, College Park, MD 20742, USA
zahra_ghasemi@yahoo.com
ASME Membership: N/A

Woongsun Jeon
Department of Mechanical Engineering, University of Minnesota, Minneapolis, MN 55455, USA
111 Church Street SE, Minneapolis, MN 55455, USA
jeonx121@umn.edu
ASME Membership: Student Member

Chang-Sei Kim
School of Mechanical Engineering, Chonnam National University, Gwangju, 61186, Korea
77 Yongbong-Ro, Buk-Gu, Gwangju 61186, South Korea
ckim@chionnam.ac.kr
ASME Membership: N/A

Anuj Gupta
Department of Medicine, University of Maryland Medical Center, Baltimore, MD 21201, USA
110 South Paca Street, 7th Floor, Cardiology, Baltimore, MD 21201
angupta@medicine.umaryland.edu
ASME Membership: N/A

Rajesh Rajamani
Department of Mechanical Engineering, University of Minnesota, Minneapolis, MN 55455, USA
111 Church Street SE, Minneapolis, MN 55455, USA
rajamani@umn.edu
ASME Membership: Fellow

Jin-Oh Hahn[1]

Department of Mechanical Engineering, University of Maryland, College Park, MD 20742, USA

2104C Glenn L. Martin Hall, University of Maryland, College Park, MD 20742, USA

Jhahn12@umd.edu

ASME Membership: Member

## ABSTRACT

*Estimating central aortic blood pressure is important for cardiovascular health and risk prediction purposes. Cardiovascular system is a multi-channel dynamical system that yields multiple blood pressures at various body sites in response to central aortic blood pressure. This paper concerns the development and analysis of an observer-based approach to de-convolution of unknown input in a class of coprime multi-channel systems applicable to non-invasive estimation of central aortic blood pressure. A multi-channel system yields multiple outputs in response to a common input. Hence, the relationship between any pair of two outputs constitutes a hypothetical input-output system with unknown input embedded as a state. The central idea underlying our approach is to derive the unknown input by designing an observer for the hypothetical input-output system. In this paper, we developed an unknown input observer (UIO) for input de-convolution in coprime multi-channel systems. We provide a universal design algorithm as well as meaningful physical insights and inherent performance limitations associated with the algorithm. The validity and potential of our approach was illustrated using a case study of estimating central aortic blood pressure waveform from two non-invasively acquired peripheral arterial pulse waveforms. The UIO could reduce the root-mean-squared error associated with the central aortic blood pressure by up to 27.5% and 28.8% against conventional inverse filtering and peripheral arterial pulse scaling techniques.*

---

[1] Department of Mechanical Engineering, University of Maryland, College Park, MD 20742, USA. Phone: +1-301-405-7864. E-mail: jhahn12@umd.edu.

## INTRODUCTION

Cardiovascular (CV) disease is a leading cause of mortality and morbidity in the United States and globally [1]. Brachial blood pressure (BP) is widely used in today's clinical practice to probe CV health and disease. But, central aortic BP measured near the heart has been suggested as superior signature of CV health and disease to conventional brachial BP [2–5]. However, direct measurement of central aortic BP involves invasive and/or inconvenient procedures and trained operators (e.g., cardiac catheterization [2,6–8] and carotid artery tonometry [9,10]), hampering its widespread use. Early efforts to overcome this obstacle was to construct a population-based mathematical transformation, called the Generalized Transfer Function (GTF) [11], which converts a peripheral (e.g., brachial [6,12,13] or radial [14–16]) arterial pulse waveform into central aortic BP waveform. The GTF is not patient-specific by nature, while the characteristics associated with the propagation of BP waves in the arteries exhibit a large degree of inter- and intra-individual variability [17]. Hence, the efficacy of the GTF technique has been controversial [18].

More recently, attempts have been made to develop patient-specific techniques for estimating central aortic BP waveform from peripheral BP waveform measurements. The vast majority of these techniques are built upon the so-called blind system identification methodology [19]. The methodology, when applied to coprime multi-channel systems with unknown input signal, determines the channel dynamics and then de-convolves the input signal by exploiting the correlation relationship between the channels. In particular, the input-deconvolution step of the methodology has employed various techniques, such as direct inverse filtering [7,20], least-squares and maximum-

likelihood-type de-convolution [21,22], and the design of dedicated de-convolution filters [23,24]. Direct inverse filtering has been a straightforward choice due to the non-minimum phase nature of the channel dynamics associated with the BP wave propagation in the arteries [25]. The least-squares and maximum likelihood-type de-convolution techniques were developed primarily for finite impulse response (FIR) channel dynamics [26,27]. Hence, central aortic BP de-convolution based on these techniques involved the FIR filter approximation of the BP propagation channel dynamics [21,22]. To relax such restrictions, design methodologies for the input de-convolution filters applicable to coprime multi-channel systems with infinite impulse response (IIR) channel dynamics have been developed [23,24,28]. However, all these techniques have a common critical weakness: the integrity of input de-convolution hinges upon the accuracy of the channel dynamics due to the open-loop nature of these techniques. Since the channel dynamics themselves are either population-based or estimated by the blind system identification methodology, the quality of the de-convolved input signal is impacted by the errors associated with the channel dynamics. In the context of estimating central aortic BP from peripheral arterial pulses, these errors ultimately boil down to errors in the clinically important characteristics in the central aortic BP waveform (e.g., systolic (SP) and pulse (PP) pressures), which can subsequently deteriorate its credibility for CV health and risk assessment.

In our endeavor to develop a novel input de-convolution technique equipped with robustness against the channel dynamics inaccuracy, we investigated the application of established state estimation techniques (i.e., the observers [29]) to input de-convolution in coprime multi-channel systems. The central idea underlying this technique is to derive

the unknown input signal by designing an observer for a hypothetical input-output system constructed using a pair of output signals in the multi-channel system. This "closed-loop" input de-convolution idea was inspired by two key observations: (i) that the relationship between any pair of two outputs constitutes a hypothetical input-output system with unknown input embedded as an estimable state; and (ii) that the observer can compensate for the adverse impact of the channel dynamics inaccuracy on the integrity of the de-convolved input signal by way of its corrective error feedback. In this paper, we developed and analyzed an unknown input observer (UIO) for input de-convolution in coprime multi-channel systems. In particular, we provide a universal design algorithm as well as meaningful physical insights and inherent performance limitations associated with the algorithm. Then, we illustrated its validity and potential using the clinically significant case study of estimating central aortic BP waveform from two non-invasively acquired peripheral arterial pulse waveforms.

This paper is organized as follows. In Section 2 (**UNKOWN INPUT OBSERVER DESIGN FOR COPRIME MULTI-CHANNEL LINEAR DYNAMICAL SYSTEMS**), a UIO for closed-loop input de-convolution in coprime multi-channel systems is developed and analyzed. In Section 3 (**OBSERVER-BASED DE-CONVOLUTION OF CENTRAL AORTIC BP WAVEFORM FROM NON-INVASIVE PERIPHERAL ARTERIAL PULSE WAVEFORMS**), the application of the UIO to the estimation of central aortic BP waveform from non-invasive peripheral arterial pulse waveforms is described in detail. In Section 4 (**RESULTS AND DISCUSSION**), the results are presented and discussed. In Section 5 (**CONCLUSIONS**), the paper is concluded with future work.

## UNKOWN INPUT OBSERVER DESIGN FOR COPRIME MULTI-CHANNEL LINEAR DYNAMICAL SYSTEMS

### Problem Formulation

Consider a multi-channel linear dynamical system in which a common yet unknown input signal generates multiple output signals (Fig. 1). It is assumed that the channels are coprime, i.e., they do not share common poles and/or zeros. The goal is to reconstruct the unknown input based on the output signals at the multiple channels. The basic idea of our approach is (i) to transform the multi-channel dynamics into an equivalent input-output dynamics in which the unknown input is cast into an internal state variable, and then (ii) to design an observer that can estimate the unknown input.

### Unknown Input Observer Design

Without any loss of generality, the UIO design problem can be solved for a two-channel system case. The results can be readily generalized and expanded to systems with >2 channels. Indeed, in systems with >2 channels, any pair of two channels in the system can be selected to design an UIO. Consider the following transfer functions associated with a two-channel system:

$$y_1(z) = G_1(z)u(z) = \frac{N_1(z)}{D_1(z)}u(z), \; y_2(z) = G_2(z)u(z) = \frac{N_2(z)}{D_2(z)}u(z) \qquad (1)$$

where $u$ is the common input, $y_1$ and $y_2$ are outputs, $G_1(z)$ and $G_2(z)$ are the channel transfer functions associated with $y_1$ and $y_2$, and $N_1(z)$, $D_1(z)$, $N_2(z)$, and $D_2(z)$ are polynomials in the discrete-time shift operator $z$ of degrees $m_1$, $n_1$, $m_2$, and $n_2$, respectively. It is assumed that $D_1(z)$ and $D_2(z)$ are monic. It is further assumed that

$m_1 = n_1$, i.e., $G_1(z)$ is a proper transfer function, and that $G_2(z)$ does not have any zeros

at the origin. Note that the properness of $G_1(z)$ is not a restriction, because any strictly

proper $G_1(z)$ can be made proper by padding z's to its numerator polynomial $N_1(z)$:

$\bar{N}_1(z) = z^{r_1} N_1(z)$, where $r_1 = n_1 - m_1$ is the relative degree of $G_1(z)$. In this way, an

equivalent input-output relationship $\bar{y}_1(z) = \bar{G}_1(z)u(z) = \frac{\bar{N}_1(z)}{D_1(z)} u(z)$ with the forward-

shifted output $\bar{y}_1(z) = y_1(z)z^{r_1}$ can be constructed. The zeros at the origin in $G_2(z)$ can

be likewise be removed by forward-shifting $y_2(z)$. Then, the unknown input $u(z)$ may be

reconstructed from $y_1(z)$ and $y_2(z)$ as follows:

Theorem 1: Consider the two-channel system in Eq. (1) with $G_1(z)$ and $G_2(z)$ given

by:

$$G_1(z) = \frac{N_1(z)}{D_1(z)} = \frac{b_{n_1}^{(1)} z^{n_1} + b_{n_1-1}^{(1)} z^{n_1-1} + \cdots + b_0^{(1)}}{z^{n_1} + a_{n_1-1}^{(1)} z^{n_1-1} + \cdots + a_0^{(1)}}, \quad G_2(z) = \frac{N_2(z)}{D_2(z)} = \frac{b_{m_2}^{(2)} z^{m_2} + b_{m_2-1}^{(2)} z^{m_2-1} + \cdots + b_0^{(2)}}{z^{n_2} + a_{n_2-1}^{(2)} z^{n_2-1} + \cdots + a_0^{(2)}}$$

$$(2)$$

which satisfy the following properties:

1) The transfer functions $G_1(z)$ and $G_2(z)$ are coprime

2) The polynomials $D_1(z)$ and $D_2(z)$ are monic

3) The transfer function $G_1(z)$ is proper and minimum phase

4) The transfer function $G_2(z)$ does not have any zero at the origin

Let $\{A_1, B_1, C_1, D_1\}$ with $D_1 = b_{n_1}^{(1)}$ and $\{A_2, B_2, C_2, D_2\}$ with $D_2 = 0$ be the controllable

canonical form realizations of $G_1(z)$ and $G_2(z)$, respectively. Then, the unknown input $u$

of this coprime multi-channel system can be reconstructed by the following UIO:

$$\hat{x}(k+1) = \bar{A}\hat{x}(k) + \bar{B}y_1(k) + \bar{L}[y_2(k) - \bar{C}\hat{x}(k)], \quad \hat{u}(k) = \frac{1}{b_{n_1}^{(1)}}[y_1(k) - \check{C}\hat{x}(k)] \quad (3)$$

where $x(k) = \begin{bmatrix} x_1(k) \\ x_2(k) \end{bmatrix}$ with $x_1$ and $x_2$ the state vectors of dimension $n_1$ and $n_2$, $\bar{A} =$

$\begin{bmatrix} A_1 - B_1C_1/b_{n_1}^{(1)} & 0_{n_1 \times n_2} \\ -B_2C_1/b_{n_1}^{(1)} & A_2 \end{bmatrix}$, $\bar{B} = \frac{1}{b_{n_1}^{(1)}}\begin{bmatrix} B_1 \\ B_2 \end{bmatrix}$, $\bar{C} = [0_{1 \times n_1} \quad C_2]$, $\check{C} = [C_1 \quad 0_{1 \times n_2}]$, and $\bar{L}$ is a

UIO gain matrix of dimension $(n_1 + n_2) \times 1$ with which all the eigenvalues of $\bar{A} - \bar{L}\bar{C}$ are

placed in the unit circle.

Proof and Analysis: The state space realization of the multi-channel system in Eq.

(1) is given by:

$$x(k+1) = \begin{bmatrix} A_1 & 0 \\ 0 & A_2 \end{bmatrix}x(k) + \begin{bmatrix} B_1 \\ B_2 \end{bmatrix}u(k), \quad \begin{bmatrix} y_1(k) \\ y_2(k) \end{bmatrix} = \begin{bmatrix} C_1 & 0 \\ 0 & C_2 \end{bmatrix}x(k) + \begin{bmatrix} b_{n_1}^{(1)} \\ 0 \end{bmatrix}u(k) \quad (4)$$

Given that $u$ is unknown but can be represented as a function of $x_1$ and $y_1$: $u(k) =$

$\frac{1}{b_{n_1}^{(1)}}[y_1(k) - C_1x_1(k)]$, Eq. (4) can be rewritten as follows:

$$x(k+1) = \begin{bmatrix} A_1 & 0 \\ 0 & A_2 \end{bmatrix}x(k) + \begin{bmatrix} B_1 \\ B_2 \end{bmatrix}u(k) = \begin{bmatrix} A_1 & 0 \\ 0 & A_2 \end{bmatrix}x(k) + \frac{1}{b_{n_1}^{(1)}}\begin{bmatrix} B_1 \\ B_2 \end{bmatrix}[y_1(k) - C_1x_1(k)]$$

$$= \bar{A}x(k) + \bar{B}y_1(k)$$

$$y_2(k) = C_2x_2(k) = \bar{C}x(k) \quad (5)$$

Hence, the UIO in Eq. (3) can reconstruct $u$ from $y_1$ and $y_2$ if the pair $(\bar{A}, \bar{C})$ is observable.

Noting that both $\{A_1, B_1, C_1, D_1\}$ and $\{A_2, B_2, C_2, D_2\}$ are associated with controllable

canonical form, we have:

$$A_1 = \begin{bmatrix} 0 & 1 & & \\ \vdots & & \ddots & \\ -a_0^{(1)} & \cdots & & -a_{n_1-1}^{(1)} \end{bmatrix}, \quad B_1 = \begin{bmatrix} 0 \\ \vdots \\ 1 \end{bmatrix}, \quad C_1 = [b_0^{(1)} - b_{n_1}^{(1)}a_0^{(1)} \quad \cdots \quad b_{n_1-1}^{(1)} - b_{n_1}^{(1)}a_{n_1-1}^{(1)}]$$

$$(6a)$$

$$A_2 = \begin{bmatrix} 0 & 1 & & \\ \vdots & & & \ddots \\ -a_0^{(2)} & \cdots & & -a_{n_2-1}^{(2)} \end{bmatrix}, \quad B_2 = \begin{bmatrix} 0 \\ \vdots \\ 1 \end{bmatrix}, \quad C_2 = \begin{bmatrix} b_0^{(2)} & \cdots & b_{m_2}^{(2)} & 0_{1\times(n_2-m_2)} \end{bmatrix}$$

(6b)

Then, it can be easily shown that $\{A_3, B_3, C_3, D_3\} = \{A_1 - B_1 C_1/b_{n_1}^{(1)}, B_1/b_{n_1}^{(1)}, -C_1/b_{n_1}^{(1)}, 1/D_1\}$ is the controllable canonical form realization of $G_1^{-1}(z)$. Indeed, using Eq. (6a):

$$A_1 - B_1 C_1/b_{n_1}^{(1)} = \begin{bmatrix} 0 & 1 & & \\ \vdots & & & \ddots \\ -\frac{b_0^{(1)}}{b_{n_1}^{(1)}} & \cdots & & -\frac{b_{n_1-1}^{(1)}}{b_{n_1}^{(1)}} \end{bmatrix} \triangleq A_3 \tag{7a}$$

$$-C_1/b_{n_1}^{(1)} = \begin{bmatrix} -\frac{b_0^{(1)}}{b_{n_1}^{(1)}} + a_0^{(1)} & \cdots & -\frac{b_{n_1-1}^{(1)}}{b_{n_1}^{(1)}} + a_{n_1-1}^{(1)} \end{bmatrix} \triangleq C_3 \tag{7b}$$

Eq. (7) yields $C_3(zI - A_3)^{-1}B_3 + D_3 = \frac{z^{n_1}+a_{n_1-1}^{(1)}z^{n_1-1}+\cdots+a_0^{(1)}}{b_{n_1}^{(1)}z^{n_1}+b_{n_1-1}^{(1)}z^{n_1-1}+\cdots+b_0^{(1)}} = G_1^{-1}(z)$. Thus, $\bar{A}$ can be rewritten as $\bar{A} = \begin{bmatrix} A_3 & 0_{n_1\times n_2} \\ B_2 C_3 & A_2 \end{bmatrix}$. Computing the observability matrix of the pair $(\bar{A}, \bar{C})$ yields:

$$\bar{O} = [O_1 \quad O_2] = \begin{bmatrix} 0_{r_2\times n_1} & C_2 \\ \vdots & C_2 A_2 \\ \sum_{i=0}^{k-r_2-1} C_2 A_2^{k-1-i} B_2 C_3 A_3^i & \vdots \\ \vdots & C_2 A_2^{n_1+n_2-1} \end{bmatrix} \tag{8}$$

where $r_2 = n_2 - m_2$ is the relative degree of $G_2(z)$ and $r_2 + 1 \leq k \leq n_1 + n_2$. Since the pair $(A_2, C_2)$ is observable, $O_2$ has full column rank, i.e., $\text{rank}(O_2) = n_2$. Further, $O_1$ reduces to the following after Gaussian elimination:

$$O_1 = \begin{bmatrix} 0_{r_2\times n_1} \\ C_3 \\ C_3 A_3 \\ \vdots \\ C_3 A_3^{n_1+n_2-r_2-1} \end{bmatrix} \tag{9}$$

which, since the pair $(A_3, C_3)$ is observable and $n_1 + n_2 - r_2 - 1 \geq n_1$, guarantees that $O_1$ has full column rank, i.e., $\text{rank}(O_1) = n_1$. Thus, $\bar{O}$ is a full rank matrix, meaning that the pair $(\bar{A}, \bar{C})$ is observable and the existence of the UIO in Eq. (3) is guaranteed.

Note that the rationale for the minimum phase requirement imposed on $G_1(z)$ is now obvious: according to Schur's determinant identity, the eigenvalues of $\overline{A}$ are given by those of $A_2$ and $A_3$:

$$\det(pI - \overline{A}) = \det(pI - A_2)\det(pI - A_3) \tag{10}$$

In addition, the eigenvalues of $A_3$ correspond to the poles of $G_1^{-1}(z)$, i.e., the zeros of $G_1(z)$.

### Intuitive Interpretation and Limiting Behavior

Intuitively, the UIO in Eq. (3) is equivalent to a Luenberger observer designed for the system with $y_1$ and $y_2$ as input and output and $u$ as an internal state, i.e., $y_2(z) = G_2(z)G_1^{-1}(z)y_1(z)$ (Fig. 2). Indeed, since $G_1(z)$ and $G_2(z)$ are coprime, a state space realization of the system is given by:

$$x_3(k+1) = A_3 x_3(k) + B_3 y_1(k), \quad u(k) = C_3 x_3(k) + D_3 y_1(k) \tag{11a}$$

$$x_2(k+1) = A_2 x_2(k) + B_2 u(k), \quad y_2(k) = C_2 x_2(k) \tag{11b}$$

where $\{A_2, B_2, C_2, D_2\}$ and $\{A_3, B_3, C_3, D_3\}$ are the controllable canonical form realization of $G_2(z)$ and $G_1^{-1}(z)$ as defined in Eq. (6) and Eq. (7). Serially concatenating Eq. (11a) and Eq. (11b) yields:

$$\begin{bmatrix} x_3(k+1) \\ x_2(k+1) \end{bmatrix} = \begin{bmatrix} A_3 & 0_{n_1 \times n_2} \\ B_2 C_3 & A_2 \end{bmatrix} \begin{bmatrix} x_3(k) \\ x_2(k) \end{bmatrix} + \begin{bmatrix} B_3 \\ B_2/b_{n_1}^{(1)} \end{bmatrix} y_1(k) \tag{12a}$$

$$y_2(k) = [0_{1 \times n_1} \quad C_2] \begin{bmatrix} x_3(k) \\ x_2(k) \end{bmatrix} \tag{12b}$$

which is identical to Eq. (5). Thus, the UIO in Eq. (3) for the plant in Eq. (5) is identical to the Luenberger observer for the plant in Eq. (12).

The above intuitive insight streamlines the analysis of the limiting behavior of the UIO with respect to the magnitude of its gain $\bar{L}$. On the one hand, if $\bar{L} \approx 0$, Eq. (3) dictates that $\hat{u}(z) = G_1^{-1}(z)y_1(z)$; indeed, when $\bar{L} \approx 0$:

$$\hat{x}_1(k+1) = A_3\hat{x}_1(k) + B_3y_1(k), \quad \hat{u}(k) = \frac{1}{b_{n_1}^{(1)}}[y_1(k) - C_1\hat{x}_1(k)] = C_3\hat{x}_1(k) + D_3y_1(k)$$

(13)

which is identical to Eq. (11a). Hence, $\hat{u}$ is essentially given by inverse filtering of $y_1(k)$ with $G_1(z)$. On the other hand, if $\bar{L} \approx \infty$, Eq. (3) dictates that $\hat{u}(z) = G_2^{-1}(z)y_2(z)$; indeed, when $\bar{L}$ is very large:

$$\hat{x}_2(k+1) = B_2C_3\hat{x}_1(k) + A_2\hat{x}_2(k) + \frac{B_2}{b_{n_1}^{(1)}}y_1(k) + L_2[y_2(k) - C_2\hat{x}_2(k)]$$

$$= B_2C_3\hat{x}_1(k) + A_2\hat{x}_2(k) + \frac{B_2}{b_{n_1}^{(1)}}[C_1\hat{x}_1(k) + D_1\hat{u}(k)] + L_2[y_2(k) - C_2\hat{x}_2(k)]$$

$$= B_2C_3\hat{x}_1(k) + A_2\hat{x}_2(k) + B_2[\hat{u}(k) - C_3\hat{x}_1(k)] + L_2[y_2(k) - C_2\hat{x}_2(k)]$$

$$= A_2\hat{x}_2(k) + B_2\hat{u}(k) + L_2[y_2(k) - C_2\hat{x}_2(k)] \tag{14}$$

In addition, very large $\bar{L}$ enforces $\hat{y}_2(k) = C_2\hat{x}_2(k) = y_2(k)$, which, in conjunction with Eq. (14), yields:

$$\hat{x}_2(k+1) \cong A_2\hat{x}_2(k) + B_2\hat{u}(k), \quad \hat{y}_2(k) = C_2\hat{x}_2(k) \tag{15}$$

which reduces to $\hat{y}_2(z) \cong G_2(z)\hat{u}(z)$, i.e., $\hat{u}$ is essentially given by inverse filtering of $y_2(k)$ with $G_2(z)$.

The above limiting behavior of the UIO provides an important insight into the fundamental limitation in its performance when applied to coprime multi-channel systems: the UIO does not provide any improvement in the accuracy of the estimated unknown input beyond open-loop inverse filtering when $\bar{L} \approx 0$ and $\bar{L} \approx \infty$. Indeed, the accuracy of

the estimated unknown input approaches to that associated with the open-loop inverse filtering of $y_1$ with $G_1(z)$ if the gain is chosen to be too small (see Eq. (13)), whereas it approaches to that associated with the open-loop inverse filtering of $y_2$ with $G_2(z)$ if the gain is chosen to be too large (see Eq. (15)). This unique limiting behavior can be attributed to the coprimeness of the channel dynamics. The plant in Eq. (5) (or equivalently, Eq. (12); also see Fig. 2) computes $u$ from $y_1$ ($u(z) = G_1^{-1}(z)y_1(z)$), and then computes $y_2$ from $u$ thus computed ($y_2(z) = G_2(z)u(z)$). Since the UIO reduces to the open-loop plant dynamics (i.e., Eq. (5)) when $\bar{L} = 0$, and $u$ can be estimated solely from $y_1$, $\hat{u}(z) = G_1^{-1}(z)y_1(z)$. On the other hand, when $\bar{L} = \infty$, the corrective error feedback acts to achieve $\tilde{y}_2 \triangleq y_2 - \hat{y}_2 = 0$. In other words, $u$ computed by the plant dynamics as $u(z) = G_1^{-1}(z)y_1(z)$ is corrected to yield $\hat{u}$ to achieve $y_2(z) = G_2(z)\,\hat{u}(z)$. Thus, in this case $u$ can be estimated solely from $y_2$, $\hat{u}(z) = G_2^{-1}(z)y_2(z)$. Given that the notion of how small or large $\bar{L}$ is depends on the channel dynamics, the appropriate range of $\bar{L}$ (i.e., the range of $\bar{L}$ that is not too small and not too large) also depends on the problem at hand.

An important practical implication of the above limiting behavior associated with the UIO is that iterative trial and error process may be required to design a UIO whose performance is superior to simple open-loop inverse filtering: in contrast to conventional observer design problems (in which corrective error feedback action can be strengthened by simply increasing the observer gain to achieve a larger improvement in closed-loop estimation relative to its open-loop counterpart), the gain of the UIO designed for coprime multi-channel systems must be carefully chosen (i.e., it must not be too small or too large) to maximize the benefit of the corrective error feedback action.

## OBSERVER-BASED DE-CONVOLUTION OF CENTRAL AORTIC BP WAVEFORM FROM NON-INVASIVE PERIPHERAL ARTERIAL PULSE WAVEFORMS

The validity, strengths, and limitations of the input de-convolution technique based on the UIO developed in this work was examined in a clinically significant real-world problem of estimating central aortic BP waveform from two non-invasively acquired peripheral arterial pulse waveform measurements (Fig. 3). Central aortic BP and pulse waveform recordings (PVR) at arm and leg sites were measured simultaneously using BP cuffs loaded at a sub-diastolic pressure level. The multi-channel artery dynamics associated with the central aortic BP-brachial PVR channel and the central aortic BP-leg PVR channel were estimated using the PVR signals [20]. Then, central aortic BP was estimated using the UIO designed based on the channel dynamics. Details follow.

### Experimental Data

The experimental central aortic BP and peripheral PVR signals were simultaneously recorded from 10 cardiac catheterization patients at the University of Maryland Medical Center under its IRB approval and written informed consent [20]. In each patient, the central aortic BP waveform was invasively measured with a catheter inserted through a femoral artery per routine standard of care, while the PVR waveforms were non-invasively measured at an upper arm and an upper leg, with occlusive BP cuffs loaded at a sub-diastolic pressure level. All the signals were stored in a laptop computer through a data acquisition system at a sampling frequency of 1 kHz for approximately 1 min. The sensors and the data acquisition system were calibrated before collecting data from each patient

to ensure the accuracy of the measurements.  The two PVR signals were used to estimate the plant dynamics as well as to design the UIO, while the central aortic BP was used to evaluate the performance of the UIO.  Table 1 shows the range of central aortic SP, PP, and mean pressures associated with the 10 patients considered in this work.  Fig. 5 presents representative measurements of (a) pulse volume recording (PVR) signals at an arm and a leg and (b) central aortic BP signal.

### Plant Dynamics: Blood Pressure Wave Propagation in Multi-Channel Arteries

The plant dynamics considered in this work involves two channels: one associated with the relationship between central aortic BP and arm PVR (C1; Fig. 3), and the other associated with the relationship between central aortic BP and leg PVR (C2; Fig. 3).  These channels are likely coprime given that they are associated primarily with arm arteries and leg arteries, respectively, whose mechanical and wave propagation properties are largely distinct [30].  Each channel dynamics is represented based on (i) a tube-load model to represent the BP wave propagation in the artery, (ii) a viscoelastic model to represent the characteristics of the arterial wall and the tissues, and (iii) a physics-based model of the BP cuff [20] (Fig. 4).  In an array of our prior work, we have shown that such a linear time-invariant representation of BP wave propagation in arteries and arterial pressure-volume relationship is valid and effective at least within a short time window (i.e., in the order of minutes) [17,20,23,31–33].    In particular, the tube-load model associated with each channel dynamics was expressed by the following discrete-time rational transfer function:

$$\mathcal{Z}[P_i(t)] = G_i(z)\mathcal{Z}[P_0(t)] = \frac{z+\theta_{1,i}+\theta_{2,i}}{z^{n_i+1}+\theta_{1,i}z^{n_i}+\theta_{2,i}z^{-n_i}}\mathcal{Z}[P_0(t)] \tag{16}$$

where $P_0(t)$ and $P_i(t)$ are the central aortic BP and the arterial BP at the peripheral site $i$ ($i = 1,2$), $\mathcal{Z}[\cdot]$ is the Z transform, and $n_i$, $\theta_{1,i}$, and $\theta_{2,i}$ are the patient-specific tube-load model parameters. In each patient, these model parameters were determined from the experimental data collected from the patient using a blind system identification procedure developed in our prior work [20]. Then, we confirmed that the rational transfer functions associated with central aortic-arm channel and central aortic-leg channel were coprime by examining the poles and zeros therein. Table 2 presents the range of the parameter values thus determined.

In the channel dynamics, the viscoelastic artery wall-tissue model and the physics-based BP cuff model are interconnected. In addition, the physics-based BP cuff model involves nonlinearity, which is not suited to the UIO design developed in this work. However, these models can be inverted, i.e., the models allow for the computation of the peripheral BP waveforms from the corresponding PVR signals (Fig. 4). Therefore, the UIO design was applied to the tube-load model component of the channel dynamics by considering the arm and leg BP waveforms estimated from the corresponding PVR signals as the outputs of the channel dynamics expressed by Eq. (16). Note that Eq. (16) meets, or can be manipulated to meet (as described in **UNKOWN INPUT OBSERVER DESIGN FOR COPRIME MULTI-CHANNEL LINEAR DYNAMICAL SYSTEMS**), all the properties listed in Theorem 1.

## Unknown Input Observer Design

For each patient, the UIO was designed using the patient-specific plant dynamics derived above and guided by Theorem 1. First, the transfer function $G_i(z)$ shown in Eq.

(16) associated with the channel $C_i$ (Fig. 3) was made proper by padding $2n_i$ forward shift operators $z$ in its numerator polynomial (both $i = 1$ and $i = 2$ were considered). Second, the controllable canonical form realizations associated with the patient-specific channel dynamics $G_1(z)$ ($\{A_1, B_1, C_1, D_1\}$) and $G_2(z)$ ($\{A_2, B_2, C_2, D_2\}$) were obtained. Third, the matrices $\bar{A}$, $\bar{B}$, $\bar{C}$, and $\check{C}$ in Eq. (3) required for the UIO design were computed using the patient-specific controllable canonical form realizations thus obtained. Finally, the UIO in Eq. (3) was constructed by designing the gain $\bar{L}$.

Considering that the primary interest of this work was to investigate the validity and potential of the UIO-based input de-convolution technique, and that the performance of the UIO approaches to open-loop inverse filtering if $\bar{L} = 0$ and $\bar{L} = \infty$, the UIO gain $\bar{L}$ was designed by trial and error to investigate if any choice of $\bar{L}$ can lead to the UIO whose input de-convolution performance is superior to open-loop inverse filtering (in terms of the discrepancy between the true versus UIO-estimated central aortic BP). Two alternative approaches were specifically employed: pole placement and linear matrix inequality (LMI).

In the pole placement approach, the Butterworth pole layout [34] was considered as the desired pole locations for the closed-loop error dynamics in the continuous-time domain. For each patient, the continuous-time Butterworth poles with unspecified cut-off frequency were calculated according to the system order (i.e., the order of Eq. (3)). Then, a large number of candidate UIO pole locations were created by varying the cut-off frequency within its maximal value dictated by the sampling frequency $F_s$ (i.e., $\frac{\pi}{F_s}$). Subsequently, these candidate pole locations were transformed into the discrete-time domain. For each candidate pole location, a candidate UIO was designed with the pole

16

placement technique [29].  The performance of the UIO was measured in terms of the root-mean-squared error (RMSE) between the true versus estimated central aortic BP waveforms.  The UIO associated with the patient (called the UIO-PP) was then determined as the one exhibiting the smallest RMSE among all the candidate UIOs.

In the LMI approach, the UIO design problem was cast into an LMI problem so that the poles associated with the closed-loop error dynamics are clustered in the region specified by $|z| < \sigma$.  In this way, the error convergence rate may be specified explicitly in the UIO design (i.e., the settling time associated with the UIO error convergence has a settling time smaller than $\frac{4}{F_s \ln \sigma}$).  Based on the UIO in Eq. (3), the error dynamics given by:

$$\tilde{x}(k + 1) = (\overline{A} - \overline{L}\overline{C})\tilde{x}(k) \tag{17}$$

According to a prior work [35], the poles of the matrix $\overline{A} - \overline{L}\overline{C}$ associated with the error dynamics in Eq. (17) can be clustered in a region if and only if there exists a symmetric positive definite matrix $P > 0$ such that:

$$\Omega_1 \otimes P + \Omega_2 \otimes [(\overline{A} - \overline{L}\overline{C})P] + \Omega_2^T \otimes [(\overline{A} - \overline{L}\overline{C})P]^T < 0 \tag{18}$$

where $\otimes$ is the Kronecker product of matrices, while $\Omega_1$ and $\Omega_2$ are square matrices that specify the region in terms of an LMI:

$$\Omega_1 + z\Omega_2 + z^*\Omega_2^T < 0 \tag{19}$$

The region specified by $|z| < \sigma$ can be expressed as the following LMI:

$$z^*z < \sigma^2 \ \rightarrow \ -\sigma + z^*(\sigma^{-1})z < 0 \ \rightarrow \ \begin{bmatrix} -\sigma & z \\ z^* & -\sigma \end{bmatrix} = \begin{bmatrix} -\sigma & 0 \\ 0 & -\sigma \end{bmatrix} + \begin{bmatrix} 0 & 1 \\ 0 & 0 \end{bmatrix}z + \begin{bmatrix} 0 & 0 \\ 1 & 0 \end{bmatrix}z^* <$$

$$0 \tag{20}$$

which implies that $\Omega_1 = \begin{bmatrix} -\sigma & 0 \\ 0 & -\sigma \end{bmatrix}$ and $\Omega_2 = \begin{bmatrix} 0 & 1 \\ 0 & 0 \end{bmatrix}$. Hence, Eq. (18) reduces to the following:

$$\Omega_1 \otimes P + \Omega_2 \otimes [(\overline{A} - \overline{L}\overline{C})P] + \Omega_2^T \otimes [(\overline{A} - \overline{L}\overline{C})P]^T$$

$$= \begin{bmatrix} -\sigma & 0 \\ 0 & -\sigma \end{bmatrix} \otimes P + \begin{bmatrix} 0 & 1 \\ 0 & 0 \end{bmatrix} \otimes [(\overline{A} - \overline{L}\overline{C})P] + \begin{bmatrix} 0 & 0 \\ 1 & 0 \end{bmatrix} \otimes [(\overline{A} - \overline{L}\overline{C})P]^T$$

$$= \begin{bmatrix} -\sigma P & (\overline{A} - \overline{L}\overline{C})P \\ P(\overline{A} - \overline{L}\overline{C})^T & -\sigma P \end{bmatrix} < 0 \tag{21}$$

Since the eigenvalues are invariant against matrix transpose, Eq. (21) can be rewritten as follows:

$$\begin{bmatrix} -\sigma P & (\overline{A}^T - \overline{C}^T\overline{L}^T)P \\ P(\overline{A} - \overline{L}\overline{C}) & -\sigma P \end{bmatrix} < 0 \tag{22}$$

Using the change of variable $K = \overline{L}^T P$, Eq. (22) becomes the following LMI:

$$\begin{bmatrix} -\sigma P & \overline{A}^T P - \overline{C}^T K \\ P\overline{A} - K^T\overline{C} & -\sigma P \end{bmatrix} < 0 \tag{23}$$

Once the matrix $K$ and $P$ satisfying Eq. (23) are found, the UIO gain $\overline{L}$ can be determined by $\overline{L} = P^{-1}K^T$.

For each patient, the UIO was designed by solving the LMI feasibility problem in Eq. (23) while varying $\sigma$ values ($0 < \sigma < 1$) to yield a large number of candidate UIOs. Similarly to the pole placement technique above, the performance of the UIO was measured in terms of the root-mean-squared error (RMSE) between the true versus estimated central aortic BP waveforms. The UIO associated with the patient (called the UIO-LMI) was then determined as the one exhibiting the smallest RMSE among all the candidate UIOs.

## Unknown Input Observer Performance Analysis

The performance of UIO-PP and UIO-LMI was measured in terms of the waveform

RMSE as well as the absolute errors associated with SP (SPE) and PP (=SP-DP; PPE) between

the true versus estimated central aortic BP waveforms.  These errors were computed for

each patient.  Then, the mean and SD were computed.

To assess the performance of the UIO in estimating central aortic BP waveform

relative to the conventional as well as primitive techniques, the same error metrics (RMSE,

SPE, and PPE) were likewise computed for the conventional open-loop inverse filtering

technique as well as the arm and leg PVR signals scaled to central aortic diastolic and mean

pressures.  For each patient, open-loop inverse filtering technique was performed by

filtering (i) the arm PVR signal by the inverse of $G_1(z)$ as well as (ii) the leg PVR signal by

the inverse of $G_2(z)$ to yield the estimated central aortic BP waveforms.  For each patient,

PVR scaling was performed by linearly calibrating the arm and leg PVR signals so that the

diastolic and mean pressure levels associated with the PVR signals become identical to the

central aortic diastolic and mean pressures measured from the patient as follows:

$$\hat{u}(t) = \frac{\overline{u} - \breve{u}}{\overline{w}_i - \breve{w}_i} w_i(t) + \frac{1}{\overline{w}_i - \breve{w}_i} (\breve{u}\overline{w}_i - \overline{u}\breve{w}_i) \tag{24}$$

where $\overline{u}$ and $\breve{u}$ are central aortic mean and diastolic pressures, while $\overline{w}_i$ and $\breve{w}_i$ are mean

and diastolic values of the PVR signal $w_i(t)$ $(i = 1,2)$.  Then, the aforementioned error

metrics between the true central aortic BP waveform versus these waveforms were

computed for each patient, whose mean and SD were subsequently computed.

Statistical significance in the difference between the error metrics associated with

UIO, open-loop inverse filtering, and scaled PVR signals was determined with the Wilcoxon

signed-rank test, where the Bonferroni correction factor of 2 was used to account for the multiple comparisons (i.e., UIO-PP versus inverse filtering and scaled PVR signals, as well as UIO-LMI versus inverse filtering and scaled PVR signals).

## RESULTS AND DISCUSSION

Table 3 summarizes RMSE, SPE, and PPE associated with central aortic BP waveforms derived from UIO-PP, UIO-LMI, open-loop inverse filtering, and scaled PVR signals, while Fig. 6 illustrates a few representative examples of true versus estimated central BP waveforms: (a) an example where UIO shows performance marginally superior to inverse filtering and (b) an example where UIO shows performance largely superior to inverse filtering.

The input de-convolution based on the UIO was in general superior to open-loop inverse filtering (which represents the limiting performance of the UIO at $\overline{L} = 0$ and $\overline{L} = \infty$) in the sense that central aortic BP waveform derived by the UIO was closer in shape to the true central aortic BP waveform than the one derived by inverse filtering. This suggests that the corrective error feedback action provided by the UIO is practically meaningful. On the average, the RMSE associated with the UIO-PP was 27.5% smaller than the open-loop inverse filtering and 28.8% smaller than the scaled arm and leg PVR signals (Table 3). Likewise, the RMSE associated with the UIO-LMI was 15.7% smaller than the open-loop inverse filtering and 17.3% smaller than the scaled arm and leg PVR signals (Table 3). In case of UIO-PP, the UIO designed with $P_1$ and $P_2$ designated as its input and output (i.e., $y_1 = P_1$ and $y_2 = P_2$ in Eq. (3); UIO-PP$_1$ in Table 3) was superior to the open-loop inverse

filtering based on both $P_1$ (i.e., $\bar{L} = 0$; $IF_1$ in Table 3) and $P_2$ (i.e., $\bar{L} = \infty$; $IF_2$ in Table 3) in all 10 patients, while the UIO designed with $P_2$ and $P_1$ designated as its input and output (i.e., $y_1 = P_2$ and $y_2 = P_1$ in Eq. (3); UIO-PP$_2$ in Table 3) was superior to the same open-loop inverse filtering (i.e., $IF_1$ and $IF_2$) in most (i.e., 8) patients. In case of UIO-LMI, the UIO designed with (i) $P_1$ and $P_2$ designated as its input and output (UIO-LIM$_1$ in Table 3) and (ii) $P_2$ and $P_1$ designated as its input and output (UIO-LMI$_2$ in Table 3) was superior to both $IF_1$ and $IF_2$ in 6 and 5 patients, respectively. In the remaining patients whose UIO did not excel both $IF_1$ and $IF_2$, the UIO exhibited a RMSE value between the RMSE values associated with $IF_1$ and $IF_2$, as predicted by the mathematical analysis presented in **Intuitive Interpretation and Limiting Behavior**. Both UIO-PP and UIO-LMI exhibited RMSE values smaller than those associated with the scaled arm and leg PVR signals in 7 and all 10 patients, respectively.

The input de-convolution based on UIO-PP also estimated central aortic SP and PP more accurately than open-loop inverse filtering and scaled PVR signals. The SPE and PPE associated with the UIO-PP were smaller than those associated with both inverse filtering and scaled PVR signals. On the average, the SPE and PPE associated with the UIO-PP were 38.1% and 45.5% smaller than open-loop inverse filtering, and 56.3% and 63.4% smaller than the scaled arm and leg PVR signals (Table 3). The SPE and PPE associated with the UIO-LMI were likewise 21.4% and 12.7% smaller than inverse filtering, and 56.0% and 41.5% smaller than the scaled arm and leg PVR signals (Table 3). This is notable in that SPE and PPE were not explicitly optimized during the UIO design process (although they may improve as the waveform accuracy is optimized). However, in contrast to UIO-PP (which yielded average SPE and PPE values smaller than the same values associated with both $IF_1$

and IF$_2$), UIO-LMI yielded average SPE and PPE values between the same values associated with IF$_1$ and IF$_2$.

Comparing UIO-PP and UIO-LMI, the UIO-PP yielded superior accuracy to the UIO-LMI. However, its design process was more ad-hoc and resource-intensive. In fact, the UIO-PP was obtained by rigorously optimizing the RMSE metric associated with the central aortic BP waveform, whereas the UIO-LMI was obtained simply by solving a LMI feasibility problem with a rudimentary constraint. It is plausible that the efficacy of the UIO-LMI may further be improved by augmenting the currently used LMI problem formulation with more stringent constraints that specify the transient and steady-state behaviors of the error convergence dynamics. Similarly, the efficacy of the UIO-PP may likewise be improved by considering a wide range of desired closed-loop pole locations. But in any case, given that the performance of the UIO-based input de-convolution technique is bounded by the open-loop inverse filtering, both design procedures may require careful selection and tuning of the observer gain.

## CONCLUSIONS

In our attempt to enable more accurate patient-specific estimation of central aortic BP waveform from non-invasively acquired peripheral arterial pulse waveforms, we developed and validated an observer-based closed-loop approach to input de-convolution in coprime multi-channel linear dynamical systems. A universal UIO design algorithm and insightful mathematical analysis were presented to elucidate key properties and inherent performance limitations of the UIO. The results obtained from the experimental data

showed promise and consistency with the mathematical analysis. The UIO presented in our work has applicability to a broad spectrum of coprime multi-channel linear systems beyond central aortic BP estimation problem. Future work includes the extension of the proposed input de-convolution algorithm to incorporate more advanced state estimation techniques with rigorous robustness guarantee against errors and uncertainties pertaining to the channel dynamics and measurement noise, as well as intensive evaluation of the algorithm in a larger datasets as well as other real-world applications.

## FUNDING

## REFERENCES

[1] Benjamin, E. J., Virani, S. S., Callaway, C. W., Chamberlain, A. M., Chang, A. R., Cheng, S., Chiuve, S. E., Cushman, M., Delling, F. N., Deo, R., De Ferranti, S. D., Ferguson, J. F., Fornage, M., Gillespie, C., Isasi, C. R., Jiménez, M. C., Jordan, L. C., Judd, S. E., Lackland, D., Lichtman, J. H., Lisabeth, L., Liu, S., Longenecker, C. T., Lutsey, P. L., MacKey, J. S., Matchar, D. B., Matsushita, K., Mussolino, M. E., Nasir, K., O'Flaherty, M., Palaniappan, L. P., Pandey, A., Pandey, D. K., Reeves, M. J., Ritchey, M. D., Rodriguez, C. J., Roth, G. A., Rosamond, W. D., Sampson, U. K. A., Satou, G. M., Shah, S. H., Spartano, N. L., Tirschwell, D. L., Tsao, C. W., Voeks, J. H., Willey, J. Z., Wilkins, J. T., Wu, J. H. Y., Alger, H. M., Wong, S. S., and Muntner, P., 2018, *Heart Disease and Stroke Statistics - 2018 Update: A Report from the American Heart Association*.

[2] Mceniery, C. M., Cockcroft, J. R., Roman, M. J., Franklin, S. S., and Wilkinson, I. B., 2014, "Central Blood Pressure: Current Evidence and Clinical Importance," Eur. Heart J., **35**, pp. 1719–1725.

[3] Ferguson, J. M., Minas, J., Siapantas, S., Komesaroff, P. A., and Sudhir, K., 2008, "Effects of a Fixed-Dose ACE Inhibitor-Diuretic Combination on Ambulatory Blood Pressure and Arterial Properties in Isolated Systolic Hypertension," J. Cardiovasc. Pharmacol., **51**(6), pp. 590–595.

[4] Roman, M. J., Okin, P. M., Kizer, J. R., Lee, E. T., Howard, B. V, and Devereux, R. B., 2010, "Relations of Central and Brachial Blood Pressure to Left Ventricular Hypertrophy and Geometry: The Strong Heart Study," J. Hypertens., **28**(2), pp. 384–388.

[5] Roman, M. J., Devereux, R. B., Kizer, J. R., Lee, E. T., Galloway, J. M., Ali, T., Umans, J. G., and Howard, B. V, 2007, "Central Pressure More Strongly Relates to Vascular Disease and Outcome Than Does Brachial Pressure: The Strong Heart Study," Hypertension, **50**, pp. 197–203.

[6] Sharman, J. E., Lim, R., Qasem, A. M., Coombes, J. S., Burgess, M. I., Franco, J., Garrahy, P., Wilkinson, I. B., and Marwick, T. H., 2006, "Validation of a Generalized Transfer Function to Noninvasively Derive Central Blood Pressure during Exercise," Hypertension, **47**(6), pp. 1203–1208.

[7] Fazeli, N., Kim, C.-S., Rashedi, M., Chappell, A., Wang, S., MacArthur, R., McMurtry, M. S., Finegan, B., and Hahn, J.-O., 2014, "Subject-Specific Estimation of Central Aortic Blood Pressure via System Identification: Preliminary In-Human Experimental Study," Med. Biol. Eng. Comput., **52**(10), pp. 895–904.

[8] Ding, F.-H., Fan, W.-X., Zhang, R.-Y., Zhang, Q., Li, Y., and Wang, J.-G., 2011, "Validation of the Noninvasive Assessment of Central Blood Pressure by the SphygmoCor and Omron Devices Against the Invasive Catheter Measurement," Am. J. Hypertens., **24**(12), pp. 1306–1311.

[9] Gallagher, D., Adji, A., and O'Rourke, M. F., 2004, "Validation of the Transfer Function Technique for Generating Central from Peripheral Upper Limb Pressure Waveform," Am. J. Hypertens., **17**(11 Pt 1), pp. 1059–67.

[10] Chen, C. H., Ting, C. T., Nussbacher, A., Nevo, E., Kass, D. A., Pak, P., Wang, S. P., Chang, M. S., and Yin, F. C., 1996, "Validation of Carotid Artery Tonometry as a Means of Estimating Augmentation Index of Ascending Aortic Pressure,"

Hypertension, **27**(2), pp. 168–175.

[11]    Chen, C. H., Nevo, E., Fetics, B., Pak, P. H., Yin, F. C., Maughan, W. L., and Kass, D. A., 1997, "Estimation of Central Aortic Pressure Waveform by Mathematical Transformation of Radial Tonometry Pressure," Circulation, **95**(7), pp. 1827–1836.

[12]    Shih, Y.-T., Cheng, H.-M., Sung, S.-H., Hu, W.-C., and Chen, C.-H., 2013, "Comparison of Two Generalized Transfer Functions for Measuring Central Systolic Blood Pressure by an Oscillometric Blood Pressure Monitor," J. Hum. Hypertens., **27**(3), pp. 204–10.

[13]    Cheng, H., Sung, S., Shih, Y., Chuang, S., Yu, W., and Chen, C., 2012, "Measurement of Central Aortic Pulse Pressure : Noninvasive Brachial Cuff-Based Estimation by a Transfer Function Vs. a Novel Pulse Wave Analysis Method," Am. J. Hypertens., **25**(11), pp. 1162–1169.

[14]    Hope, S. A., Meredith, I. T., Tay, D., and Cameron, J. D., 2007, "'Generalizability' of a Radial-Aortic Transfer Function for the Derivation of Central Aortic Waveform Parameters," J. Hypertens., **25**(9), pp. 1812–1820.

[15]    Cameron, J. D., McGrath, B. P., and Dart, A. M., 1998, "Use of Radial Artery Applanation Tonometry and a Generalized Transfer Function to Determine Aortic Pressure Augmentation in Subjects with Treated Hypertension.," J. Am. Coll. Cardiol., **32**(5), pp. 1214–20.

[16]    Chen, C.-H., Nevo, E., Fetics, B., Pak, P. H., Yin, F. C. P., Maughan, W. L., and Kass, D. A., 1997, "Estimation of Central Aortic Pressure Waveform by Mathematical Transformation of Radial Tonometry Pressure," Circulation, **95**(7), pp. 1827–1836.

[17]    Rashedi, M., Fazeli, N., Chappell, A., Wang, S., MacArthur, R., McMurtry, M. S., Finegan, B. a, and Hahn, J. O., 2013, "Comparative Study on Tube-Load Modeling of Arterial Hemodynamics in Humans," ASME J. Biomech. Eng., **135**(March), p. 31005.

[18]    Hope, S. A., Tay, D. B., Meredith, I. T., and Cameron, J. D., 2003, "Use of Arterial Transfer Functions for the Derivation of Aortic Waveform Characteristics," J. Hypertens., **21**(7), pp. 1299–1305.

[19]    Abed-Meraim, K., Qiu, W., and Hua, Y., 1997, "Blind System Identification," Proc. IEEE, **85**(8), pp. 1310–1322.

[20]    Ghasemi, Z., Kim, C., Ginsberg, E., Gupta, A., and Hahn, J.-O., 2017, "Model-Based Blind System Identification Approach to Estimation of Central Aortic Blood Pressure Waveform from Noninvasive Diametric Circulatory Signals," J. Dyn. Syst. Meas. Control, **139**(June), p. Article 061003.

[21]    Swamy, G., Ling, Q., Li, T., and Mukkamala, R., 2007, "Blind Identification of the Aortic Pressure Waveform from Multiple Peripheral Artery Pressure Waveforms," Am. J. Physiol. Heart Circ. Physiol., **292**(5), pp. H2257-64.

[22]    Abutaleb, A. S., Waheed, M. E.-S., and Elhamy, N. M., 2010, "Multichannel Blind Deconvolution Using the Stochastic Calculus for the Estimation of the Central Arterial Pressure," Math. Probl. Eng., **2010**, pp. 1–21.

[23]    Hahn, J.-O., Reisner, A. T., and Asada, H. H., 2009, "Blind Identification of Two-Channel IIR Systems With Application to Central Cardiovascular Monitoring," J. Dyn. Syst. Meas. Control, **131**, p. 051009.

[24]    Hahn, J. O., McCombie, D. B., Reisner, A. T., Hojman, H. M., and Harry, A., 2010,

"Identification of Multichannel Cardiovascular Dynamics Using Dual Laguerre Basis Functions for Noninvasive Cardiovascular Monitoring," IEEE Trans. Control Syst. Technol., **18**(1), pp. 170–176.

[25] Zhang, G., Hahn, J. O., and Mukkamala, R., 2011, "Tube-Load Model Parameter Estimation for Monitoring Arterial Hemodynamics," Front. Physiol., **2 NOV**(November), pp. 1–18.

[26] Hua, Y., 2002, "Blind Methods of System Identification," Circuits, Syst. Signal Process., **21**(1), pp. 91–108.

[27] Alberge, F., Duhamel, P., and Nikolova, M., 2002, "Adaptive Solution for Blind Identification / Equalization Using Deterministic Maximum Likelihood," IEEE Trans. Signal Process., **50**(4), pp. 923–936.

[28] Gürelli, M. L., and Nikias, C. L., 1995, "EVAM: An Eigenvector-Based Deconvolution of Input Colored Signals," IEEE Tran. Signal Process., **43**(1), pp. 134–149.

[29] Chen, C. T., 1998, *Linear System Theory and Design*, Oxford University Press, New York.

[30] Buntin, C. M., and Silver, F. H., 1990, "Noninvasive Assessment of Mechanical Properties of Peripheral Arteries," Ann. Biomed. Eng., **18**, pp. 549–566.

[31] Ghasemi, Z., Lee, J. C., Kim, C. S., Cheng, H. M., Sung, S. H., Chen, C. H., Mukkamala, R., and Hahn, J. O., 2018, "Estimation of Cardiovascular Risk Predictors from Non-Invasively Measured Diametric Pulse Volume Waveforms via Multiple Measurement Information Fusion," Sci. Rep., **8**(1), p. Article 10433.

[32] Fazeli, N., Kim, C. S., Rashedi, M., Chappell, A., Wang, S., MacArthur, R., McMurtry, M. S., Finegan, B., and Hahn, J. O., 2014, "Subject-Specific Estimation of Central Aortic Blood Pressure via System Identification: Preliminary in-Human Experimental Study," Med. Biol. Eng. Comput., **52**(10), pp. 895–904.

[33] Abdollahzade, M., Kim, C.-S., Fazeli, N., Finegan, B. A., Sean McMurtry, M., and Hahn, J.-O., 2014, "Data-Driven Lossy Tube-Load Modeling of Arterial Tree: In-Human Study," J. Biomech. Eng., **136**(10), p. 101011.

[34] Franklin, G. F., Powell, J. D., and Emami-Naeini, A., 1994, *Feedback Control of Dynamic Systems*, Pearson Higher Education, Inc., Upper Saddle River.

[35] Chilali, M., and Gahinet, P., 1996, "H_∞ Design with Pole Placement Constraints: An LMI Approach," IEEE Trans. Automat. Contr., **41**(3), pp. 358–367.

Figure Captions List

Fig. 1            A coprime multi-channel linear dynamical system in which a common yet unknown input signal $u(z)$ generates multiple output signals $y_1(z)$ and $y_2(z)$.

Fig. 2            A hypothetical input-output system derived from a coprime multi-channel system by designating its one output signal as input to the hypothetical input-output system and its another output signal as output of the same system.

Fig. 3            Observer-based de-convolution of central aortic blood pressure (BP) waveform from non-invasive peripheral arterial pulse waveform measurements.  The pulse volume waveform recordings (called PVR) are made at the upper arm and leg sites using the BP cuffs loaded at a sub-diastolic pressure level.  These diametric PVR signals are applied to a system identification procedure[20] to derive the channel dynamics associated with (i) the propagation of the BP wave from the aorta to the peripheral arteries and (ii) the propagation and distortion of the peripheral BP waves into the PVR signals at the respective peripheral measurement sites.  The unknown input observer (UIO) designed using the estimated channel dynamics estimates central aortic BP from peripheral PVR signals.

Fig. 4            Multi-channel wave propagation dynamics in the arteries represented by (i) a tube-load model to represent the BP wave propagation in the artery,

(ii) a viscoelastic model to represent the characteristics of the arterial wall and the tissues, and (iii) a physics-based model of the BP cuff.

Fig. 5    Representative measurements of (a) pulse volume recording (PVR) signals at an arm and a leg and (b) central aortic blood pressure (BP) signal.

Fig. 6    Representative examples of true versus estimated central BP waveforms: (a) an example where UIO-PP shows performance marginally superior to inverse filtering and (b) an example where UIO-PP shows performance largely superior to inverse filtering.

## Table Caption List

Table 1    The range of central aortic systolic (SP), pulse (PP), and mean (MP) pressures associated with 10 cardiac catheterization patients.

Table 2    The range of tube-load model parameters associated with 10 cardiac catheterization patients.

Table 3    The root-mean-squared errors (RMSEs), systolic pressure errors (SPEs), and pulse pressure errors (PPEs) associated with central aortic blood pressure waveforms derived from UIO-PP, UIO-LMI, open-loop inverse filtering (IF), and scaled PVR signals (N=10).  UIO-PP: UIO designed with pole placement. UIO-LMI: UIO designed with LMI.

$$G_1(z)=N_1(z)/D_1(z) \longrightarrow y_1(z)$$

$$G_2(z)=N_2(z)/D_2(z) \longrightarrow y_2(z)$$

$u(z)$

○
○
○

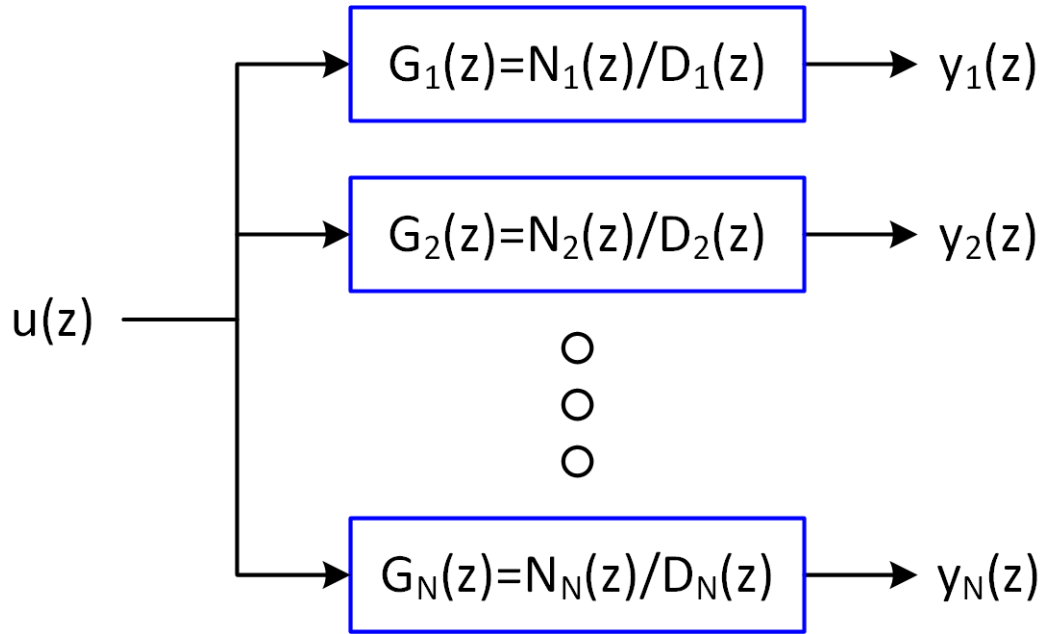$$G_N(z)=N_N(z)/D_N(z) \longrightarrow y_N(z)$$

Fig. 1: A coprime multi-channel linear dynamical system in which a common yet unknown input signal $u(z)$ generates multiple output signals $y_1(z)$ and $y_2(z)$.
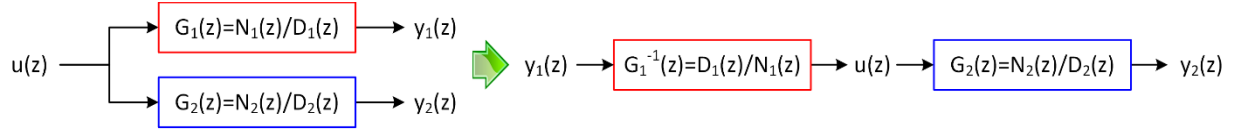
**Fig. 2**: A hypothetical input-output system derived from a coprime multi-channel system by designating its one output signal as input to the hypothetical input-output system and its another output signal as output of the same system.
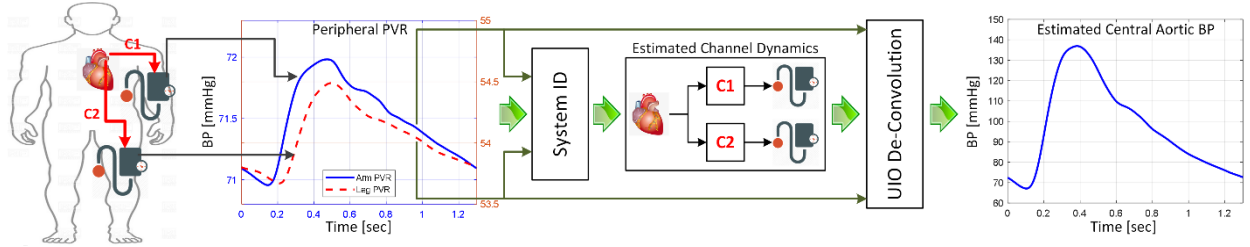
Fig. 3: Observer-based de-convolution of central aortic blood pressure (BP) waveform from non-invasive peripheral arterial pulse waveform measurements. The pulse volume waveform recordings (called PVR) are made at the upper arm and leg sites using the BP cuffs loaded at a sub-diastolic pressure level. These diametric PVR signals are applied to a system identification procedure[20] to derive the channel dynamics associated with (i) the propagation of the BP wave from the aorta to the peripheral arteries and (ii) the propagation and distortion of the peripheral BP waves into the PVR signals at the respective peripheral measurement sites. The unknown input observer (UIO) designed using the estimated channel dynamics estimates central aortic BP from peripheral PVR signals.
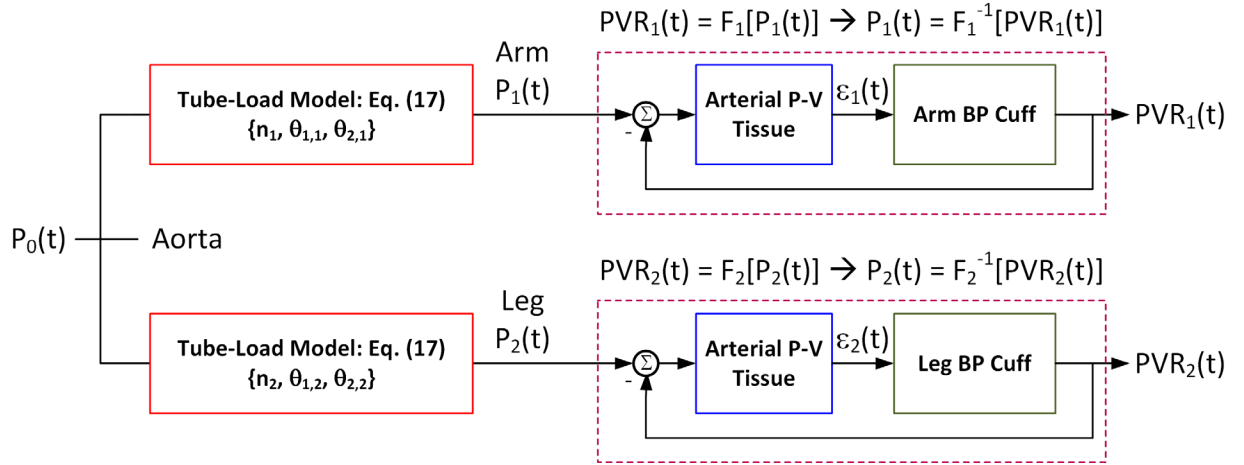
Fig. 4: Multi-channel wave propagation dynamics in the arteries represented by (i) a tube-load model to represent the BP wave propagation in the artery, (ii) a viscoelastic model to represent the characteristics of the arterial wall and the tissues, and (iii) a physics-based model of the BP cuff.
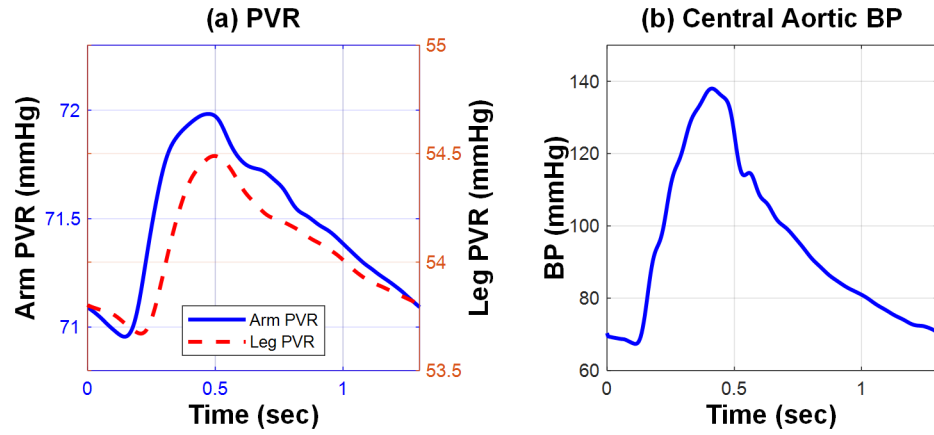
Fig. 5: Representative measurements of (a) pulse volume recording (PVR) signals at an arm and a leg and (b) central aortic blood pressure (BP) signal.
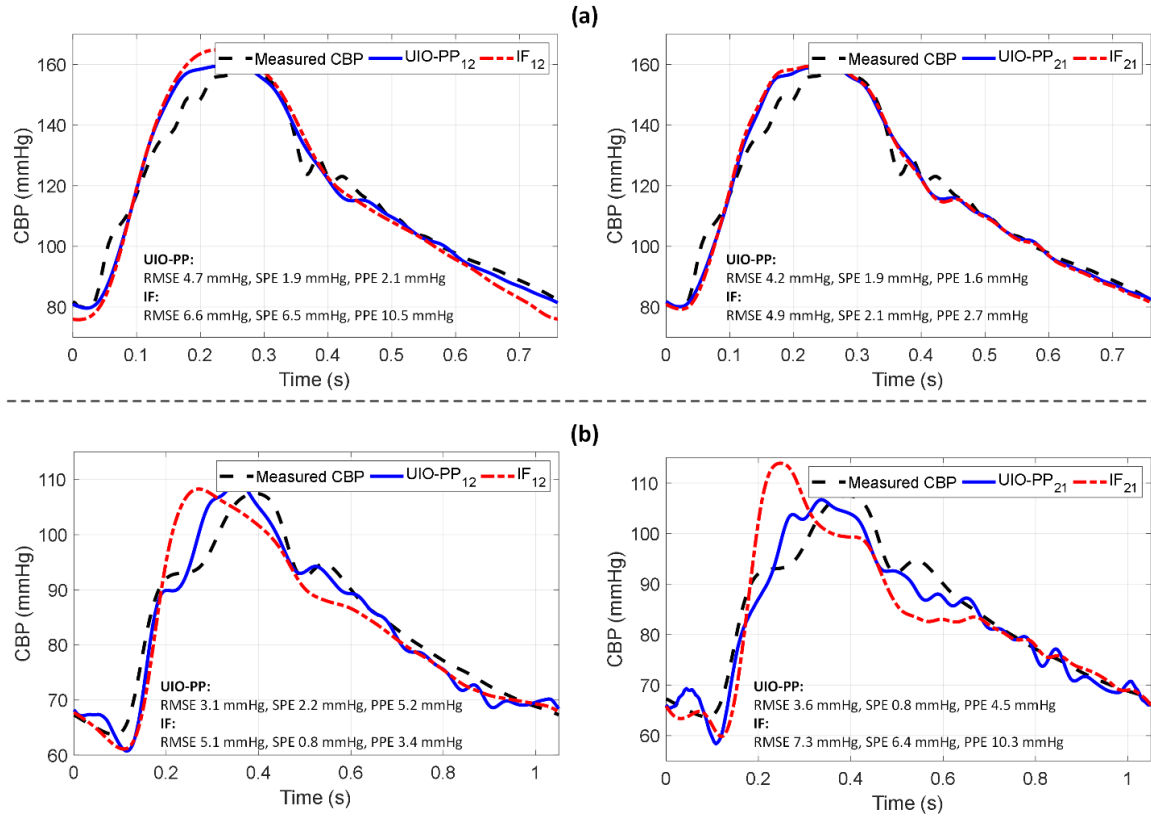
**Fig. 6**: Representative examples of true versus estimated central BP waveforms: (a) an example where UIO-PP shows performance marginally superior to inverse filtering and (b) an example where UIO-PP shows performance largely superior to inverse filtering.

Table 1: The range of central aortic systolic (SP), pulse (PP), and mean (MP) pressures associated with 10 cardiac catheterization patients (mean+/-SD).

| SP [mmHg] | PP [mmHg] | MP [mmHg] |
| --- | --- | --- |
| 126+/-26 | 54+/-20 | 95+/-20 |

Table 2: The range of tube-load model parameters associated with 10 cardiac catheterization patients.

| Channel 1 (Upper Arm) | | | Channel 2 (Upper Leg) | | |
|---|---|---|---|---|---|
| $n_1$ | $\theta_{1,1}$ | $\theta_{2,1}$ | $n_2$ | $\theta_{1,2}$ | $\theta_{2,2}$ |
| 2-18 | 56.1-294.0 | 0.01-18.6 | 7 - 24 | 3.4-500.2 | 0.01-249.1 |

Table 3: The root-mean-squared errors (RMSEs), systolic pressure errors (SPEs), and pulse pressure errors (PPEs) associated with central aortic blood pressure waveforms derived from UIO-PP, UIO-LMI, open-loop inverse filtering (IF), and scaled PVR signals (N=10). UIO-PP: UIO designed with pole placement. UIO-LMI: UIO designed with LMI.

(a) UIO-PP

|  | UIO-PP$_1$ ($y_1 = P_1$) | UIO-PP$_2$ ($y_1 = P_2$) | Average |
|---|---|---|---|
| RMSE [mmHg] | 3.7+/-1.7 | 3.6+/-1.0 | 3.7+/-1.4*† |
| SPE [mmHg] | 2.7+/-2.0 | 2.4+/-1.6 | 2.6+/-1.7† |
| PPE [mmHg] | 3.2+/-3.4 | 2.9+/-1.9 | 3.0+/-2.7*† |

*: p<0.025 with respect to inverse filtering (Wilcoxon signed-rank test).
†: p<0.025 with respect to scaled PVR signals (Wilcoxon signed-rank test).

(b) UIO-LMI

|  | UIO-LMI$_1$ ($y_1 = P_1$) | UIO-LMI$_2$ ($y_1 = P_2$) | Average |
|---|---|---|---|
| RMSE [mmHg] | 4.2+/-2.0 | 4.4+/-1.7 | 4.3+/-1.8* |
| SPE [mmHg] | 3.4+/-3.1 | 3.3+/-2.0 | 3.3+/-2.6† |
| PPE [mmHg] | 4.8+/-4.1 | 4.9+/-3.4 | 4.8+/-3.7 |

*: p<0.025 with respect to inverse filtering (Wilcoxon signed-rank test).
†: p<0.025 with respect to scaled PVR signals (Wilcoxon signed-rank test).

(c) Inverse Filtering

|  | IF$_1$ ($y_1 = P_1$) | IF$_2$ ($y_1 = P_2$) | Average |
|---|---|---|---|
| RMSE [mmHg] | 5.3+/-2.4 | 4.9+/-1.9 | 5.1+/-2.1 |
| SPE [mmHg] | 5.5+/-4.7 | 2.8+/-2.2 | 4.2+/-3.9 |
| PPE [mmHg] | 7.2+/-5.1 | 3.9+/-4.3 | 5.5+/-4.9 |

(d) Scaled PVR Signals

|  | Arm PVR | Leg PVR | Average |
|---|---|---|---|
| RMSE [mmHg] | 4.6+/-1.8 | 5.8+/-2.6 | 5.2+/-2.3 |
| SPE [mmHg] | 8.8+/-6.2 | 6.2+/-5.8 | 7.5+/-6.0 |
| PPE [mmHg] | 7.7+/-6.3 | 8.8+/-9.2 | 8.2+/-7.7 |